Measurements and analyses of the distribution of the radioactivity induced by the secondary neutrons produced by 17-MeV protons in compact cyclotron facility

Norihiro Matsuda[1,*], *Yuichi* Izumi[2], *Yoshiyuki* Yamanaka[2], *Toshiyuki* Gandou[2], *Masaaki* Yamada[2], and *Koji* Oishi[2]

[1]Japan Atomic Energy Agency, 2-4 Shirakata, Tokai-mura, Naka-gun, Ibaraki, Japan
[2]Japan Environment Research Co., Ltd, 6-24-1 Nishishinjyuku, Shinjyuku, Tokyo, Japan

Abstract. Measurements of reaction rates by secondary neutrons produced from beam losses by 17-MeV protons are conducted at a compact cyclotron facility with the foil activation method. The experimentally obtained distribution of the reaction rates of ^{197}Au (n, γ) ^{198}Au on the concrete walls suggests that a target and an electrostatic deflector as machine components for beam extraction of the compact cyclotron are principal beam loss points. The measurements are compared with calculations by the Monte Carlo code: PHITS. The calculated results based on the beam losses are good agreements with the measured ones within 21%. In this compact cyclotron facility, exponential attenuations with the distance from the electrostatic deflector in the distributions of the measured reaction rates were observed, which was looser than that by the inverse square of distance.

1 Introduction

Recently, high-energy electron linear accelerators for external beam therapy (EBT) for tumor treatment and compact cyclotrons to produce radiotracers for the positron emission tomography (PET) have been increasing in the medical field. There are over 1,200 accelerators in Japan as of March, 2015 according to statistics [1]. Lifetime of the accelerators is expected about 20 years [2]. There will surely come a day to replace the existing accelerator with newer models or decommission the facility itself. When the accelerator is replaced or the facility is decommissioned, we need to evaluate the total amount of radioactivity (inventory) induced by the day-to-day accelerator operations. Wastes arising during the replacing and decommissioning process aren't always radioactive wastes because clearance criteria have been introduced in regulations of Japan since 2012. We can substantially reduce the amount of radioactive waste, especially for several thousands of m^3 of concrete, by release from regulatory control based on the clearance criteria. Thus, recognizing and separating the radioactive wastes depending on the radioactivity or concentration of radioactivity is of the upmost importance to reduce the amount of those and to save the cost. There are only several reports before 2012 on the decommissioning for those accelerator facilities in Japan [3]-[7].

In planning process of the decommissioning, we also need to estimate exposure dose by gamma-rays from the radioactive nuclides induced by accelerator operations for workers engaged in the decommissioning operations in advance. Spatial distributions of ambient dose equivalent rates are measured on a periodic basis at some representative points. The information based on measurements will be available for the dose estimations. However, the spatial distributions of ambient dose equivalent rates are easily and drastically changed with time by the progress of decommissioning operations and physical decay of radioactive nuclides. The relatively high-activated accelerator and the components should be transported to off-site for reducing radiation exposure and keeping them as low as reasonable achievement. On the other hand, the radioactivity in their surrounding structure such as concrete walls is relatively low compared to that in the accelerator. For the concrete, long-half-life radioactive nuclides such as ^{152}Eu, ^{154}Eu, ^{60}Co, produced from minute impurities may become a problem for the dose estimations [2]. It can't be expected to reduce the ambient dose equivalent rates by physical decay during the decommissioning process. And it is hard to remove them to off-site without dismantling them. Therefore, we must estimate the exposure dose for workers in different situations throughout the entire period.

Thus, useful tools are required to evaluate the radioactivity and estimate the ambient dose equivalent rates in accelerator facility explained above. Particle and Heavy Ion Transport code System, PHITS [8], coupled with high energy particle induced radioactivity calculation code, DCHAIN-SP 2001 [9] (hereinafter called PHITS-DCHAIN), is prepared in the package of the PHITS which is available from the Organization for Economic Cooperation and Development/Nuclear Energy Agency (OECD/NEA) databank [10]. The

* Corresponding author: matsuda.norihiro@jaea.go.jp

evaluation procedures for the accelerator facility with the PHITS-DCHAIN are as follows:

(i) Evaluation of average fluxes of secondary neutrons generated from beam losses during beam operation at targets, injection/extraction apparatus, dumps etc.,

(ii) Evaluation of induced radioactivity in materials after the beam operation based on the average neutron fluxes obtained above, and

(iii) Evaluation of ambient dose equivalent rates by gamma-rays from the radionuclides obtained above.

Hence, these evaluations depend on the assumption of the beam losses. These calculations are started from the beam losses. The principal beam losses in the accelerator facility, such as targets, collimators, and beam dumps are well-known as beam current to keep radiation safety and to protect accelerators. The beam current is measured from the electric and magnetic fields created by the beam. For large-scale facilities, beam loss monitors and radiation monitors are installed throughout the facility, and are used for detecting uncontrolled losses. On the other hand, most small-scale facilities for medical purposes don't have such monitors. Therefore, additional measurements are needed to understand more about the beam losses and the positions for such facilities. The PHITS-DCHAIN would be available for deducing the beam losses from the additional measurements, such as ambient dose equivalent rates, induced radioactivity, or neutron fluxes.

In this study, measurements of secondary neutrons on the concrete walls generated from beam losses are carried out with the foil activation method in a compact cyclotron facility. The measured results are compared with calculations using PHITS-DCHAIN. The characteristics of distributions of the secondary neutron flux in the facility are identified through the measurements and the analyses.

2 Methods

2.1. Arrangement of compact cyclotron facility

Figure 1 shows a top cross-sectional view of the compact cyclotron facility. There is a cyclotron (BC-1710: The Japan Steel Works, Ltd.) and it has two beam transport lines (X- and Y-course). This compact cyclotron can accelerate protons up to 17 MeV, deuterons up to 10 MeV/u, Helium-3 up to 26 MeV/u, and Helium-4 up to 20 MeV/u. The X-course is a straight-line which lies on the middle of the facility, 7.2 m extended from the cyclotron. The Y-course is a branched line by switching magnet (SM) at a 35 degrees angle in the middle of the straight-line, of which length is 4.5 m. A target, a collimator and a Faraday cup are put in a target chamber connected at the end of both beam transport lines.

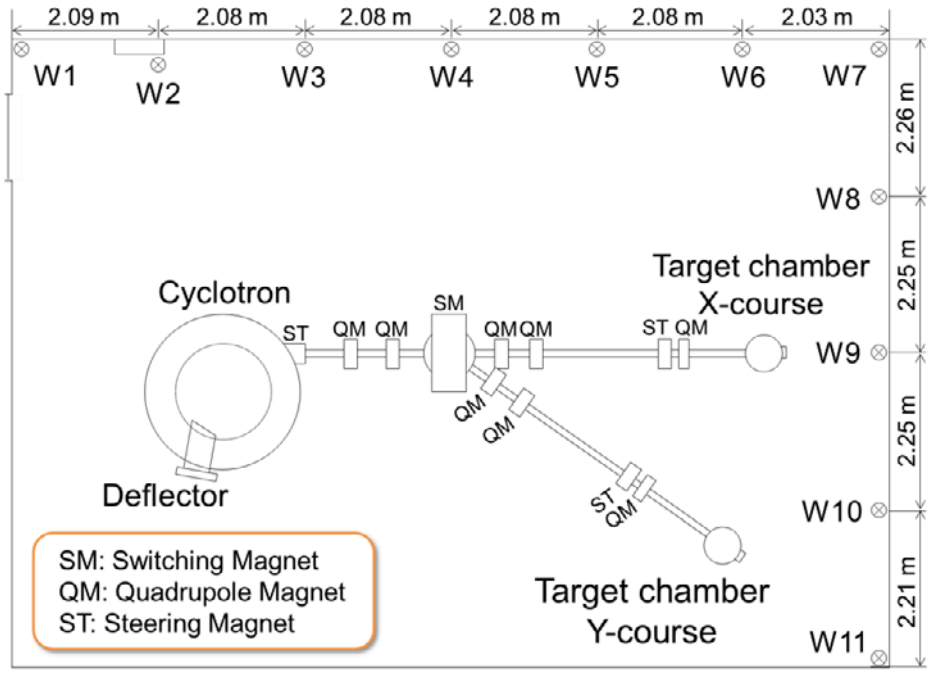

Figure 1. Top cross-sectional view of a compact cyclotron facility, which have a cyclotron, two beam transport lines and target chambers (X- and Y-course), and some magnets.

2.2. Irradiation target on X-course

During beam operation in this study, 17-MeV protons were transported only to the X-course (not transported to the Y-course). The proton beam was shaped by passing through the beam slit (collimator) of graphite (3 mm thick) with a slit aperture in the central, of which height was 10 mm and width was 5 mm. The shaped beam was impinged on the aluminum filter (0.05 mm thick), the irradiation target of SS316 (10 mm height × 5 mm width × 0.15 mm thick), and the Faraday cup (dump) of graphite (3 mm thick). These positions of beam losses from the beam slit to the Faraday cup in the target chamber, shown in Fig. 2 are hereinafter collectively called the X-target.

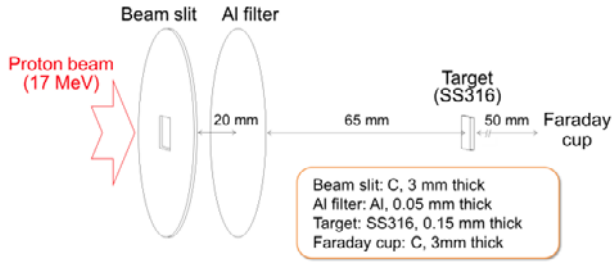

Figure 2. Arrangement of a beam slit (3 mm), an aluminum filter (0.05 mm), a SS316 target (0.15 mm) and a Faraday cup (3 mm), which are collectively called the X-target at the end of beam transport line (X-course).

2.3. Beam current to the X-target

Beam operating time of the cyclotron was 3 hours in this study. The average beam current transported to the X-target was 14.5 μA. And, the average beam current lost by the SS316 target was 1.9 μA. The beam losses at the beam slit, the aluminum filter, the SS316 target, and the Faraday cup were calculated with PHITS-DCHAIN. The calculated beam loss ratios were 77%, 0.01%, 12%, and 12%, respectively. Thus, the calculated beam losses at the SS316 target corresponded to 1.7 μA.

2.4. Beam losses at an electrostatic deflector

In a typical compact cyclotron with an electrostatic deflector for beam extraction, about 50% of accelerating protons would be lost by the electrostatic deflector [11]. The electrostatic deflector, which made from phosphorus deoxidation copper (Cu, > 99.90%) should be considered as beam loss point in this study. Since we can't directly obtain the beam current at the electrostatic deflector, the average one lost by the electrostatic deflector was estimated by beam current at beam probes A and B (shown in Fig. 3), and to the X-target. During a beam commissioning operation, the beam current at beam probes A and B was 4.8 and 3.0 μA, respectively, and that to the X-target was 2.3 μA. In this compact cyclotron, it was found that 38% of accelerating beam was lost in the vacuum chamber (between the beam probes A and B). Normalization coefficient was about 0.3 for estimating the beam current lost by the electrostatic deflector from that to the X-target. The estimated average beam current lost by the electrostatic deflector was 4.4 μAv (= 14.5 μA × 0.3). The beam losses at the electrostatic deflector were about 2.6 times larger than those at the SS316 target.

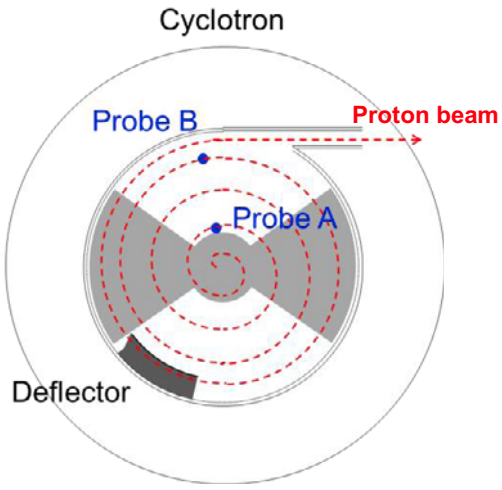

Figure 3. Arrangement of an electrostatic deflector, and beam probes (A and B) in a vacuum chamber of the compact cyclotron.

2.5. Uncontrolled losses

Uncontrolled losses may be occurred by operation failure around the beam lines such as quadrupole magnets (QM), steering magnets (ST) and switching magnet (SW) in Fig. 1. These uncontrolled beam losses kept to low level took no thought in this study. The accelerating beam loss in the vacuum chamber didn't also consider because of low-energy.

2.6. Activation measurements

Activation foils (0.02 mm thick Gold) were installed on concrete walls at the same level as the beam line (1.3 m height above the floor) shown as W1 to W11 in Fig. 1. The W1 to W11 were divided into two sides to the beam direction on X-course: left side wall (from W1 to W7) and front side wall (from W7 to W11).

After the beam operation to the X-target, the gamma-ray spectra from the activation foils were measured with the high-purity germanium (HPGe) detector (ORTEC: GMX-20195-S). The reaction rates of ^{197}Au (n, γ) ^{198}Au, which could be expressed in produced ^{198}Au atoms per target atom per incident proton, are determined after being corrected to take into account the beam current fluctuation during the irradiation. The peak efficiency of the HPGe detectors was determined by using the Gamma

Studio software of ORTEC. The components of estimated errors in reaction rates were the counting statistics and the detector efficiency.

3 Results and discussion

3.1. Experimental results

Measured reaction rates of ^{197}Au (n, γ) ^{198}Au on the concrete walls (from W1 to W11 in Fig. 1) are listed in Table 1 and showed in Fig. 4. In the figure, two peaks are observed at W2 (broad) and W7 (sharp). The reaction rate at W2 shows the largest value among all measurements. The value at W2 is 1.5 times larger than that at W7, which is the least value. On the other hand, the value at W9 clearly shows a peak on the front side wall (from W7 to W11), which is 1.3 times larger than two ends of that (W7 and W11). This result indicates that there are one or more principal beam loss points (at least two beam loss points from the number of peaks in the figure, such as around the compact cyclotron and the target chamber of the X-course).

Table 1. Measured reaction rates of ^{197}Au (n, γ) ^{198}Au on the concrete walls in the cyclotron facility.

Position	Reaction rate (atom^{-1} proton^{-1})
W1	$9.03\times10^{-18} \pm 7.10\times10^{-19}$
W2	$9.50\times10^{-18} \pm 7.11\times10^{-19}$
W3	$8.30\times10^{-18} \pm 7.01\times10^{-19}$
W4	$7.89\times10^{-18} \pm 6.55\times10^{-19}$
W5	$6.69\times10^{-18} \pm 5.59\times10^{-19}$
W6	$5.57\times10^{-18} \pm 5.25\times10^{-19}$
W7	$5.60\times10^{-18} \pm 5.30\times10^{-19}$
W8	$6.24\times10^{-18} \pm 5.87\times10^{-19}$
W9	$8.76\times10^{-18} \pm 6.90\times10^{-19}$
W10	$7.00\times10^{-18} \pm 6.10\times10^{-19}$
W11	$5.79\times10^{-18} \pm 5.72\times10^{-19}$

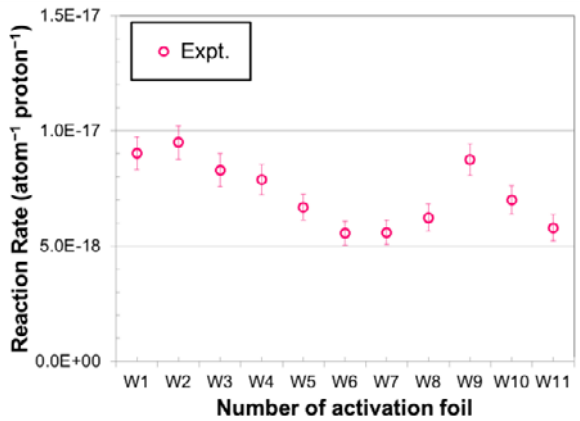

Figure 4. Distributions of measured reaction rates of ^{197}Au (n, γ) ^{198}Au on concrete walls at the same level as beam transport line (1.3 m height above the floor).

3.2 Calculation results

The experimental data on the concrete walls were compared with calculation results by using PHITS-DCHAIN adopting the Japanese Evaluated Nuclear Data Library (JENDL) -4.0 cross-section library [12]. In the calculation, the cyclotron facility including material compositions, beam energy, beam current (beam losses), and beam radius (1.1 cm) on the X-course, were precisely modelled. Absorption cross-section data of ^{197}Au (n, γ) ^{198}Au based on the JENDL dosimetry file [13] was used to convert from the calculated neutron fluxes with PHITS-DCHAIN to the reaction rates, listed in Table 2. The statistical errors (uncertainties) of calculation results for neutron transport calculations were far lower than 10%.

Table 2. Absorption cross-section data of ^{197}Au (n, γ) ^{198}Au used as conversion coefficient to the reaction rates

Reaction rate			
Energy (MeV)	Cross-section (cm^{-2})	Energy (MeV)	Cross-section (cm^{-2})
1.00×10^{-10}	8.756×10^{-23}	7.43×10^{-1}	8.498×10^{-26}
4.14×10^{-7}	2.583×10^{-23}	9.07×10^{-1}	8.036×10^{-26}
1.12×10^{-6}	2.563×10^{-23}	1.11×10^{0}	7.807×10^{-26}
2.38×10^{-6}	1.295×10^{-22}	1.35×10^{0}	6.973×10^{-26}
5.04×10^{-6}	3.058×10^{-22}	1.65×10^{0}	6.089×10^{-26}
1.07×10^{-5}	1.813×10^{-24}	2.02×10^{0}	4.954×10^{-26}
2.26×10^{-5}	1.711×10^{-23}	2.46×10^{0}	3.631×10^{-26}
1.01×10^{-4}	1.115×10^{-23}	3.01×10^{0}	2.513×10^{-26}
4.54×10^{-4}	1.126×10^{-23}	3.68×10^{0}	1.423×10^{-26}
1.58×10^{-3}	3.676×10^{-24}	4.49×10^{0}	6.204×10^{-27}
3.35×10^{-3}	1.741×10^{-24}	5.49×10^{0}	2.502×10^{-27}
7.10×10^{-3}	1.060×10^{-24}	6.70×10^{0}	8.175×10^{-28}
1.50×10^{-2}	7.005×10^{-25}	8.19×10^{0}	1.624×10^{-28}
3.18×10^{-2}	4.647×10^{-25}	1.00×10^{1}	2.756×10^{-29}
8.65×10^{-2}	3.216×10^{-25}	1.22×10^{1}	2.862×10^{-30}
1.50×10^{-1}	2.659×10^{-25}	1.35×10^{1}	8.036×10^{-31}
2.24×10^{-1}	2.152×10^{-25}	1.49×10^{1}	3.194×10^{-31}
3.34×10^{-1}	1.568×10^{-25}	1.75×10^{1}	1.060×10^{-31}
4.98×10^{-1}	1.122×10^{-25}	1.96×10^{1}	---

Calculated results of the reaction rates on the concrete walls were shown in Fig. 5 with the measured ones. Contributions for the reaction rates from the beam losses at the electrostatic deflector (blue dashed line) were larger than those at the X-target (red dotted line) on the whole, and accounted for nearly 90% of the measured ones except for ones at W9 and W10. The calculated total reaction rates (summation of the both, black solid line) were good agreements with the measured ones within 21% (C/Es: 0.91~1.21).

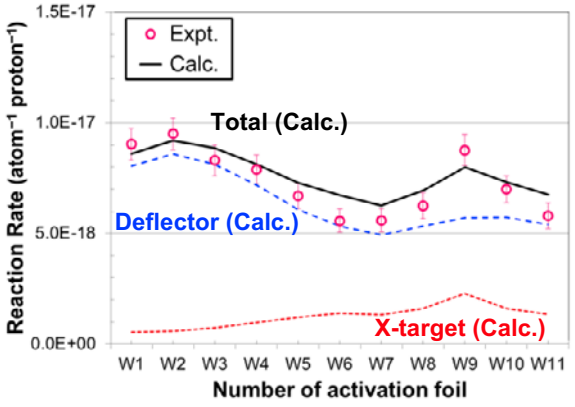

Figure 5. Distributions of measured reaction rates of ^{197}Au (n, γ) ^{198}Au on concrete walls, and calculated ones from beam losses at the X-target (red dotted line), the electrostatic deflector (blue dashed line), and the total (summation of the both, black solid line).

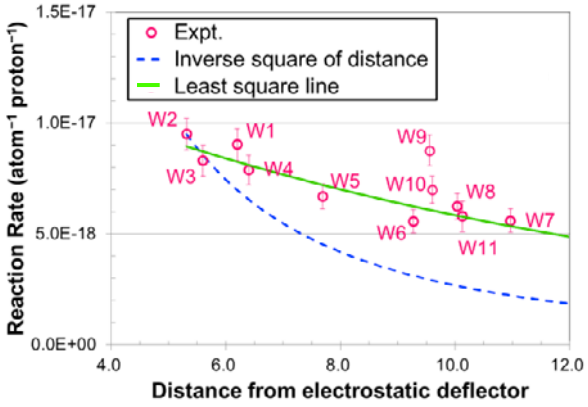

Figure 6. Distributions of measured reaction rates of ^{197}Au (n, γ) ^{198}Au on concrete walls with distance from the electrostatic deflector and the fitting line obtained by inverse square of distance (blue dashed line) and least-square method, except for that at W9 and W10 (green solid line).

3.3 Distributions of measured reaction rates in the facility

According to the calculations results of the reaction rates by PHITS-DCHAIN, secondary neutrons produced from the beam losses at the electrostatic deflector are dominant in this facility, except for ones at W9 and W10. We assume the electrostatic deflector as principal isotropic source of the secondary neutrons. Figure 6 shows distribution of the measured reaction rates with the distance from the electrostatic deflector. If there is an isotropic source, distributions of measured reaction rates will be inversely proportional to the square of the distance from the electrostatic deflector. However the distributions of measured reaction rates disagreed with the attenuation curve by the inverse square of distance from the electrostatic deflector (blue dashed line), exponential attenuation with the distance was observed (green solid line). The attenuation curve was obtained by the method of least squares, except for the measured reaction rates at W9 and W10. The attenuation curve of the measured reaction rates was looser than that by the inverse square of distance. This tendency about the exponential attenuations with the distance may make the evaluation for distributions of radioactivity and ambient dose equivalent rates in the compact cyclotron facility much easier.

4 Conclusion

The measurements on the concrete walls of the reaction rates of ^{197}Au (n, γ) ^{198}Au with the foil activation method have been carried out in the facility having the compact cyclotron with the electrostatic deflector. In this study, secondary neutrons in the facility were produced by 17-MeV protons transported to the target chamber of the X-course and from the beam losses at the electrostatic deflector during the accelerator operation. The measured data indicated that at least two beam loss points existed not only at the irradiation target but also around the compact cyclotron. The distributions of the measured reaction rates were calculated by using the PHITS-DCHAIN adopting the JENDL-4.0 cross-section library. The calculated results were good agreement with the measured ones within 21% (0.91~1.21). Moreover, it was found that the distributions of the measured reaction rates except for W9 and W10 showed exponential attenuation with the distance from the electrostatic deflector. The attenuation curve obtained by the method of least squares was looser than that by the inverse square of distance. This tendency about the distributions may make the evaluation of radioactivity and ambient dose equivalent rates in the compact cyclotron facility much easier. We need to investigate further identifying the distribution of the measured reaction rates, beam losses in the compact cyclotron facility.

Acknowledgements

We wish to thank Dr. K. Suyama for his support and advice on this study, and Dr. H. Nakashima for his help on establishing this study.

References

1. Japan radioisotope association, Statistics on the use of radiation in Japan 2015 (2016), http://www.jrias.or.jp/report/pdf/riyoutoukei2015.pdf
2. International atomic energy agency, Cyclotron produced radionuclides: guidelines for setting up a facility, International atomic energy agency technical reports series No. 471, (2009).
3. A. Endo, Dismantling work of the JAERI electron linac and measurement of induced radionuclides, J. Health Phys., 34, 161-165 (1999) in Japanese.
4. A. Yamadera, Dismantling work of cyclotron of Tohoku University and measurement of induced radionuclides, J. Health Phys., 34, 166-170 (1999) in Japanese.
5. T. Ishimoto, H. Kubota, T. Mori, K. Terakawa, K. Tani and K. Ishii, Decommissioning of the Medical Compact cyclotron, Journal of the RANDEC, 31, 21-31 (2005) in Japanese with English summary.
6. K. Masumoto, Decommissioning of accelerator facility – Example of the Tanashi branch, High Energy Accelerator Research Organization, 39, 30-43 (2009) in Japanese with English summary.
7. K. Ito, Y. Nakata, H. Matsuda and N, Sato, Decommissioning of the Medical cyclotron in National Center of Neurology and Psychiatry, Kakuigaku, 48, 109-119 (2011) in Japanese with English summary.
8. T. Sato, K. Niita, N. Matsuda, S. Hashimoto, Y. Iwamoto, S. Noda, T. Ogawa, H. Iwase, H. Nakashima, T. Fukahori, K. Okumura, T. Kai, S. Chiba, T. Furuta and L. Sihver, Particle and Heavy Ion Transport Code System PHITS, Version 2.52, J. Nucl. Sci. Technol. **50**, 913-923 (2013).
9. T. Kai, F. Maekawa, K. Kosako, Y. Kasugai, H. Takada, and Y. Ikeda, *DCHAIN-SP 2001: High energy particle induced radioactivity calculation code*, JAERI-Data/Code 2001-016, (2001). [in Japanese]
10. http://www.oecd-nea.org/tools/abstract/detail/nea-1857/
11. Y. Kumada, *Challenges to compact cyclotron*, Radiation & Industries 102, 30-35 (2004). [in Japanese]
12. K. Shibata, O. Iwamoto, T. Nakagawa, N. Iwamoto, A. Ichihara , S. Kunieda, S. Chiba, K. Furutaka, N. Otuka, T. Ohsawa, T. Murata, H. Matsunobu, A. Zukeran, S. Kamada, and J. Katakura, JENDL-4.0: A New Library for Nuclear Science and Engineering, J. Nucl. Sci. Technol. **48**, 1-30 (2011).
13. K. Kobayashi, T. Iguchi, S. Iwasaki, T. Aoyama, S. Shimakawa, Y. Ikeda, N. Odano K. Sakurai, K. Shibata, T. Nakagawa and M. Nakazawa, *JENDL Dosimetry file 99 (JENDL/D-99)*, JAERI 1344, (2002).